Dalton Transactions

Accepted Manuscript

This article can be cited before page numbers have been issued, to do this please use: J. P. Costes, F. Dahan, L. Vendier, S. Sova, G. Lorusso and M. Evangelisti, *Dalton Trans.*, 2017, DOI: 10.1039/C7DT04293K.

ROYAL SOCIETY OF CHEMISTRY

rsc.li/dalton

View Article Online
DOI: 10.1039/C7DT04293K

Journal Name

ARTICLE

Ni^{II}-Ln^{III} complexes with o-vanillin as main ligand: syntheses, structures, magnetic and magnetocaloric properties

Received 00th January 20xx,
Accepted 00th January 20xx

DOI: 10.1039/x0xx00000x

www.rsc.org/

Jean-Pierre Costes,[a,b*] Françoise Dahan,[a,b] Laure Vendier,[a,b] Sergiu Shova,[c] Giulia Lorusso,[d] Marco Evangelisti [d,e*]

Ortho-vanillin in presence of nickel and lanthanide ions yields three types of heteronuclear Ni^{II}-Gd^{III} complexes, going from dinuclear to tetranuclear defect dicubane complexes, as demonstrated by their structural determinations. These complexes are dependent on the solvents used during the reaction processes and on the retained lanthanide ions, characterized by an increase of their Lewis acid character on going from lighter to heavier lanthanide ions. Intramolecular ferromagnetic Ni^{II}-Gd^{III} interactions are present in the heterodinuclear Ni^{II}-Gd^{III} entities, while ferromagnetic Ni^{II}-Ni^{II} and Ni^{II}-Gd^{III} interactions dominate above 2 K in the tetranuclear Ni^{II}_2-Gd^{III}_2 compounds, devoid of any Gd^{III}-Gd^{III} interaction. The effect of a magnetic field on the magnetic entropy and adiabatic temperature changes is maximum near the liquid-helium boiling temperature, mainly determined by the relatively weak strength of the magnetic interactions.

Introduction

During the last two decades, several heteronuclear 3d-4f complexes have been prepared with the use of Schiff base ligands derived from ortho-vanillin (o-vanH).[1-6] The Schiff base ligands have two coordination sites of different sizes and affinities, so that the 3d ions prefer to enter into the inner N_2O_2 site, while the 4f ions are attracted by the outer O_2O_2 coordination site. Therefore, a unique main ligand is able to associate two different ions, which is interesting. Ortho-vanillin is a commercial ligand and, as salicylaldehyde,[7,8] two ligands in a *trans* arrangement are able to chelate 3d ions.[9] Ortho-vanillin can also yield 4f complexes, as a trinuclear Gd^{III} complex[10] or equivalent trinuclear Dy^{III} complexes,[11] which were studied for their interesting single-molecule magnet (SMM) properties.[12,13] In view of these previous studies, ortho-vanillin must also yield heterodinuclear 3d-4f complexes and the first examples involved Cu^{II}-Ln^{III},[14,15] Co^{II}-Ln^{III} and Ni^{II}-Ln^{III} complexes.[16,17] Two o-van ligands are needed to isolate heterodinuclear complexes after rearrangement of these ligands in a *cis* position that allows formation of two oxygenated coordination sites of different sizes. In the case of Ni^{II}-Ln^{III} complexes, our previous work demonstrated that isolation of heterodinuclear Ni^{II}-Ln^{III} complexes implying two o-van ligands is straightforward only with lighter Ln ions, the reactions becoming more puzzling with Gd^{III} ions and heavier Ln^{III} ions. More surprising rearrangements have been observed thanks to structural determinations with Y ions.[17] In a recent work, we reported on the structural determinations of original tetranuclear Co^{II}_2-Ln^{III}_2 (Ln^{III} = Gd^{III}, Tb^{III}, Y^{III}) entities showing defect-dicubane structures.[18] In view of these results, we decided to reinvestigate the chemistry of Ni^{II}-Ln^{III} complexes prepared with use of the commercial o-vanH ligand.

The research in molecular complexes containing gadolinium is particularly appealing and rewarding due to the physical properties of these materials, especially with reference to their potential application in magnetic refrigeration.[19] Gadolinium has zero orbital angular momentum and the largest entropy single ion. These conditions favor the occurrence of a large magnetocaloric effect (MCE), that is, the changes of magnetic entropy ΔS_m and adiabatic temperature ΔT_{ad}, following a change of the applied magnetic field ΔH. This effect can be exploited for implementing a refrigeration cycle. Therefore, gadolinium is the most widespread element among magnetic refrigerant materials.[20] We report hereafter the structural determinations, magnetic studies and magnetocaloric effects of some of the heterometallic Ni^{II}-Ln^{III} derived from the simple o-vanH ligand.

Experimental Section

Materials

The metal salts, $Ni(CH_3COO)_2{\cdot}4H_2O$, $Gd(NO_3)_3{\cdot}6H_2O$, $Tb(NO_3)_3{\cdot}6H_2O$, $Y(NO_3)_3{\cdot}6H_2O$, and ortho-vanillin (Aldrich) were used as purchased while $Ni(o\text{-}van)_2(H_2O)_2$ was prepared as

[a] Laboratoire de Chimie de Coordination du CNRS, 205, route de Narbonne, BP 44099, F-31077 Toulouse Cedex 4, France.
[b] Université de Toulouse; UPS, INPT, F-31077 Toulouse Cedex 4, France.
[c] "Petru Poni" Institute of Macromolecular Chemistry, Aleea Gr. Ghica Voda 41 A, Iasi 700487, Romania.
[d] Instituto de Ciencia de Materiales de Aragón (ICMA), CSIC – Universidad de Zaragoza, 50009 Zaragoza, Spain.
[e] Donostia International Physics Center (DIPC), 20018 Donostia-San Sebastián, Spain.

Electronic Supplementary Information (ESI) available: Molecular structures, magnetization and entropy data. CCDC 1053697, 1581923, 1581924, 1581926 to 1581928. For ESI and crystallographic data in CIF format, see DOI: 10.1039/x0xx00000x

View Article Online
DOI: 10.1039/C7DT04293K

previously described in MeOH/H_2O solution (3/1 ratio).[17] High-grade solvents were used for preparing the complexes.

Complex

The reactions described below are very similar for they imply the same reactants. In order to avoid repetition of the standard conditions, we insist on the differences introduced in each synthesis, differences mainly coming from the solvents used in each trial.

$[Ni(o\text{-}van)_2(H_2O)_2Gd(NO_3)_3]$ 1. Addition of $Gd(NO_3)_3{\cdot}6H_2O$ (0.43 g, 1 mmol) to a stirred suspension of $Ni(o\text{-}van)_2(H_2O)_2$ (0.4 g, 1 mmol) in acetone (20 mL) induced dissolution of the nickel(II) complex. Diffusion of diethyl ether into the filtered acetone solution yielded crystals suitable for XRD in low yield (0.11 g, 15 %). Anal. Calcd. for $C_{16}H_{18}GdN_3NiO_{17}$ (740.3): C, 26.0; H, 2.5; N, 5.7. Found: C, 26.1; H, 2.3; N, 5.3. IR (ATR): 3576w, 3447m, 3388w, 1625s, 1610m, 1557w, 1470m, 1451s, 1430m, 1301s, 1283s, 1207s, 1171w, 1094w,1065w, 1031w, 949m, 855w, 814w, 785w, 732m, 650w cm^{-1}.

$[Ni(o\text{-}van)_2(H_2O)_2Ce(NO_3)_3]$ 2. The experiment was repeated with $Ce(NO_3)_3{\cdot}6H_2O$ instead of $Gd(NO_3)_3{\cdot}6H_2O$. The resulting solution was heated for 15 min, then filtered after cooling and concentrated to half-volume. Slow evaporation yielded crystals suitable for XRD in good yield (0.50 g, 70 %). Anal. Calcd. for $C_{16}H_{18}CeN_3NiO_{17}$ (723.1): C, 26.6; H, 2.5; N, 5.8. Found: C, 26.3; H, 2.3; N, 5.5. IR (ATR): 3573w, 3436m, 3388w, 1626s, 1609m, 1554w, 1471m, 1451s, 1428m, 1298s, 1277s, 1211s, 1170w, 1095w,1065w, 1027m, 949m, 854w, 814w, 786w, 733m, 651w cm^{-1}.

$[Ni(o\text{-}van)_2(iPrOH)_2Tb(NO_3)_3]$ 3. Addition of $Tb(NO_3)_3{\cdot}6H_2O$ (0.43 g, 1 mmol) to a stirred suspension of $Ni(o\text{-}van)_2(H_2O)_2$ (0.4 g, 1 mmol) in acetone (20 mL) induced dissolution of the nickel complex. Isopropyl alcohol (20 mL) was then added and the resulting solution was filtered and kept undisturbed until green crystals suitable for XRD appeared. These crystals are very unstable out of their solution and the yield is low, 0.16 g (20 %). Anal. Calcd. for $C_{22}H_{30}N_3NiO_{17}Tb$ (826.1): C, 32.0; H, 3.7; N, 5.1. Found: C, 31.7; H, 3.5; N, 4.7. IR (ATR): 3434l, 1624s, 1611m, 1557m, 1508w, 1473m, 1451s, 1430s, 1304s, 1283s, 1210s, 1173w, 1096w,1067w, 1027w, 949m, 856w, 814w, 782w, 733m, 647w cm^{-1}.

$[Ni(o\text{-}van)_2(iPrOH)(H_2O)Gd(NO_3)_3]$ 4. Use of similar experimental conditions and $Gd(NO_3)_3{\cdot}6H_2O$ (0.43 g, 1 mmol) instead of $Tb(NO_3)_3{\cdot}6H_2O$ yielded a solution that was stirred and heated for 30 min and then concentrated to yield a green precipitate that was filtered off and dried. Yield: 0.41 g (53 %). Anal. Calcd. for $C_{19}H_{24}GdN_3NiO_{17}$ (782.3): C, 29.2; H, 3.1; N, 5.4. Found: C, 29.3; H, 2.8; N, 5.1. IR (ATR): 3403m, 1624s, 1611m, 1557w, 1501m, 1451s, 1420s, 1305m, 1273s, 1211s, 1172w, 1094w,1068w, 1025w, 951m, 855w, 814w, 781w, 730m, 649w cm^{-1}.

$[Ni(o\text{-}van)_2(CH_3CN)(H_2O)Gd(NO_3)_3]$ 5. Working in acetonitrile as a solvent yielded a green powder after heating (30 min) and stirring. Recrystallization from acetonitrile yielded crystals suitable for XRD. Yield: 0.38 g (50 %). Anal. Calcd. for $C_{18}H_{19}GdN_4NiO_{16}$ (763.3): C, 28.3; H, 2.5; N, 7.3. Found: C, 28.2; H, 2.6; N, 7.0. IR (ATR): 3423m, 1624s, 1611m, 1552w, 1451s, 1413m, 1328s, 1286s, 1210s, 1205s, 1096w,1062w, 1046w, 1028w, 951m, 856w, 816w, 742w, 728m, 650w cm^{-1}.

$[Ni(o\text{-}van)_2(\mu\text{-}NO_3)(CH_3OH)Tb(o\text{-}van)(NO_3)]H_2O$ 6. A mixture of $Ni(o\text{-}van)_2(H_2O)_2$ (0.4 g, 1 mmol) and $Tb(NO_3)_3{\cdot}6H_2O$ (0.45 g, 1 mmol) in methanol (10 mL) was heated and stirred for 20 min, yielding a green solution that was filtered off after cooling and concentrated to half-volume. Addition of isopropyl alcohol (5 mL) and slow evaporation yielded crystals suitable for XRD. Yield: 0.25 g (30 %). Anal. Calcd. for $C_{25}H_{25}N_2NiO_{16}Tb$ (827.1): C, 36.3; H, 3.0; N, 3.4. Found: C, 35.9; H, 3.1; N, 3.0. IR (KBr): 3373m, 1628s, 1552m, 1545m, 1475m, 1453m, 1432m, 1408s, 1312m, 1295m, 1245m, 1210s, 1170w, 1093w,1066w, 1050w, 1029w, 1019w, 950m, 859w, 810w, 782w, 745w, 733m, 651 cm^{-1}.

$[Gd(o\text{-}van)_2(NO_3)_2Ni(OH)(OMe)Ni(o\text{-}van)_2Gd(NO_3)_2]$ CH_3COCH_3 7. A mixture of $Ni(o\text{-}van)_2(H_2O)_2$ (0.4 g, 1 mmol) and $Gd(NO_3)_3{\cdot}6H_2O$ (0.45 g, 1 mmol) in methanol (20 mL) was heated and stirred for 1 h, yielding a green solution that was filtered off after cooling and concentrated to half-volume. Diffusion of acetone into the resulting solution yielded crystals suitable for XRD. Yield: 0.12 g, 17 %. Anal. Calcd. for $C_{36}H_{38}Gd_2N_4Ni_2O_{27}$ (1390.6): C, 31.1; H, 2.7; N, 4.0. Found: C, 30.9; H, 2.6; N, 3.8. IR (ATR): 3452w, 1703w, 1637s, 1607m, 1554w, 1470m, 1442s, 1409m, 1294s, 1239m, 1208s, 1170w, 1097w, 1066w, 1027w, 946m, 857w, 815w, 781w, 741w, 727m, 651w cm^{-1}.

$[Gd(o\text{-}van)_2(NO_3)_2Ni(OH)_2Ni(o\text{-}van)_2Gd(NO_3)_2](CH_3COCH_3)_2$ 8. Making the reaction in acetone and heating till a precipitate appears gives a complex in which only hydroxo bridges are present. Yield: 0.32 g, 45 %. Anal. Calcd. for $C_{38}H_{42}Gd_2N_4Ni_2O_{28}$ (1434.6): C, 31.8; H, 2.9; N, 3.9. Found: C, 31.9; H, 2.7; N, 3.5. IR (ATR): 3450m, 1709m, 1643s, 1610m, 1553w, 1468m, 1445s, 1417m, 1299s, 1239m, 1210s, 1167w, 1095w, 1070w, 1032w, 951m, 859w, 815w, 787w, 742w, 727m, 649w cm^{-1}.

$[Gd(o\text{-}van)_2(NO_3)_2Ni(OMe)_2Ni(o\text{-}van)_2Gd(NO_3)_2]$ 9. If dry methanol (10 mL) was used, the final precipitate corresponds to the previous one in which hydroxo bridges are replaced by methoxo bridges. Yield: 0.24 g, 35 %. Anal. Calcd. for $C_{34}H_{34}Gd_2N_4Ni_2O_{26}$ (1346.5): C, 30.3; H, 2.5; N, 4.2. Found: C, 30.3; H, 2.5; N, 3.9. IR (ATR): 1638s, 1608m, 1556w, 1471m, 1445s, 1410m, 1295s, 1239m, 1210s, 1171w, 1098w, 1068w, 1026w, 947m, 858w, 816w, 782w, 742w, 728m, 652w cm^{-1}.

$[Y(o\text{-}van)_2(NO_3)_2Ni(OH)_2Ni(o\text{-}van)_2Y(NO_3)_2]$ 10. Use of 95 % ethanol and $Y(NO_3)_3.6H_2O$ gave a complex that analyzed as a tetranuclear hydroxo bridged unit. Yield: 0.18 g, 27 %. Anal. Calcd. for $C_{32}H_{30}N_4Ni_2O_{26}Y_2$ (1297.9): C, 35.2; H, 3.3; N, 4.3. Found: C, 34.9; H, 3.1; N, 3.9. IR (ATR): 3603m, 1636s, 1609m, 1555w, 1508m, 1488m, 1472m, 1442s, 1409m, 1299s, 1242m, 1210s, 1168w, 1095w, 1067w, 1032w, 946m, 858w, 814w, 784w, 728w, 651w cm^{-1}.

Physical measurements

Elemental analyses were carried out at the Laboratoire de Chimie de Coordination Microanalytical Laboratory in Toulouse, France, for C, H, and N. IR spectra were recorded on

View Article Online
DOI: 10.1039/C7DT04293K

a Spectrum 100 FT-IR Perkin-Elmer spectrophotometer using the ATR mode. Magnetic data were obtained with a Quantum Design MPMS SQUID susceptometer. Magnetic susceptibility measurements were performed on polycrystalline samples fixed by Eicosane wax in the 2-300 K temperature range in a 0.1 T applied magnetic field. Diamagnetic corrections were applied by using Pascal's constants.[21] Isothermal magnetization measurements were performed up to 5 T at 2 K. The magnetic susceptibilities have been computed by exact calculations of the energy levels associated to the spin Hamiltonian through diagonalization of the full matrix with a general program for axial and rhombic symmetries,[22] and the magnetizations with the MAGPACK program package.[23] Least-squares fittings were accomplished with an adapted version of the function-minimization program MINUIT.[24] Heat capacity data were collected in the temperature range 0.3-20 K by using a Quantum Design PPMS, equipped with a ^{3}He cryostat. The polycrystalline samples were pressed in thin pellets with mass of about 0.5 mg. Apiezon-N grease was used to facilitate the thermalization of the samples at low temperature, and its contribution to the heat capacity was subtracted using a phenomenological expression.

Crystallographic Data Collections and Structure Determinations for (1), (2), (3), (5), (6) and (7)

Crystals of **1**, **2**, **3**, **5**, **6** and **7** were kept in the mother liquor until they were dipped into oil. The chosen crystals were mounted on a Mitegen micromount and quickly cooled down to 130 K (**1**), 160 K (**5**) or 180 K (**6**, **7**), except for (**2**, **3**) that were measured at 293 K. The selected crystals of **1** (light green, 0.35×0.2×0.05 mm^3), **2** (light green, 0.5×0.35×0.3 mm^3), **3** (green, 0.35×0.075×0.075 mm^3), **5** (green, 0.5×0.4×0.3 mm^3), **6** (yellow green, 0.35×0.2×0.05 mm^3) and **7** (light green, 0.18×0.12×0.02 mm^3) were mounted on a Xcalibur Oxford Diffraction diffractometer (**1**), an Enraf-Nonius CAD4 (**2**, **3**), a STOE-IPDS (**5**, **6**), or on a Bruker Kappa Apex II (**7**) using a graphite-monochromated Mo-Kα radiation (λ = 0.71073Å) and equipped with an Oxford Instrument Cooler Device. The unit cell determination and data integration were carried out using CrysAlis RED, Xred or SAINT packages.[25-28] The reflections were corrected for Lorentz-polarization effects with the MolEN package[29] and semi-empirical absorption corrections based on ψ scans were applied for the CAD4 measurements.[30] The structures have been solved by Direct Methods using SHELXS97[31] or SIR92,[32] and refined by means of least-squares procedures on a F^2 with the program SHELXL97[33] included in the software package WinGX version 1.63.[34] Atomic Scattering Factors were taken from International tables for X-Ray Crystallography.[33] All non-hydrogen atoms were anisotropically refined, and all hydrogen atoms were refined by using a riding model. Drawings of molecules are performed with the programs ZORTEP[35] and ORTEP3 with 30% probability displacement ellipsoids for non-hydrogen atoms.[36] CIF data for **1**, **2**, **3**, **5**, **6** and **7** have been deposited at CCDC with references CCDC 1053697, 1581923, 1581924, 1581926 to 1581928.

Crystal data for 1: $C_{16}H_{18}GdN_3NiO_{17}$, M = 740.29, monoclinic, $P2_1/c$, Z = 4, a = 9.3439(5), b = 18.1612(7), c = 14.3985(7) Å, α = γ = 90°, β = 106.594(6)°, V = 2341.63(19) Å^3, 16403 collected reflections, 4277 unique reflections (R_{int} = 0.0308), R-factor = 0.0208, weighted R-factor = 0.0492 for 3735 contributing reflections [I > 2σ (I)]. CCDC1581928.

Crystal data for 2: $C_{16}H_{18}CeN_3NiO_{17}$, M = 723.16, monoclinic, $P2_1/c$, Z = 4, a = 9.4537(6), b = 18.3586(14), c = 14.5970(12) Å, α = γ = 90°, β = 106.503(6)°, V = 2429.0(3) Å^3, 6185 collected reflections, 5853 unique reflections (Rint = 0.0123), R-factor = 0.0209, weighted R-factor = 0.0577 for 4602 contributing reflections [I > 2σ(I)]. CCDC1581927.

Crystal data for 3: $C_{22}H_{30}N_3NiO_{17}Tb$, M = 826.12, monoclinic, $P2_1/c$, Z = 4, a = 9.5216(19), b = 16.757(3), c = 19.565(4) Å, α = γ = 90°, β = 93.34 (3)°, V = 3116.3(11) Å^3, 25121 collected reflections, 7149 unique reflections (Rint = 0.062), R = 0.0349, weighted R-factor = 0.0481 for 5037 contributing reflections [I > 2σ(I)]. CCDC1581926.

Crystal data for 5: $C_{18}H_{19}GdN_4NiO_{16}$, M = 763.33, monoclinic, $P2_1/c$, Z = 4, a = 9.9098(14), b = 15.519(2), c = 16.211(2) Å, α = γ = 90°, β = 94.695 (15)°, V = 2484.6(6) Å^3, 17331 collected reflections, 3917 unique reflections (Rint = 0.0258), R = 0.0349, weighted R-factor = 0.0481 for 3765 contributing reflections [I > 2σ(I)]. CCDC1053697.

Crystal data for 6: $C_{25}H_{25}N_2NiO_{16}Tb$, M = 827.10, monoclinic, $P2_1/n$, Z = 4, a = 11.1842(11), b = 15.6136(13), c = 16.5063(14) Å, α = γ = 90°, β = 90.277 (11)°, V = 2882.4(4) Å^3, 28070 collected reflections, 5523 unique reflections (Rint = 0.0475), R = 0.0316, weighted R-factor = 0.0673 for 4117 contributing reflections [I > 2σ(I)]. CCDC1581924.

Crystal data for 7: $C_{36}H_{37}Gd_2N_4Ni_2O_{27}$, M = 1389.62, triclinic, P-1, Z = 1, a = 10.7627(5), b = 11.1417(5), c = 12.7244(6) Å, α = 73.703(2)°, β = 66.381 (2)°, γ = 64.462(2)°, V = 1250.65(10) Å^3, 19324 collected reflections, 5063 unique reflections (Rint = 0.0251), R = 0.0505, weighted R-factor = 0.173 for 4117 contributing reflections [I > 2σ(I)]. CCDC1581923.

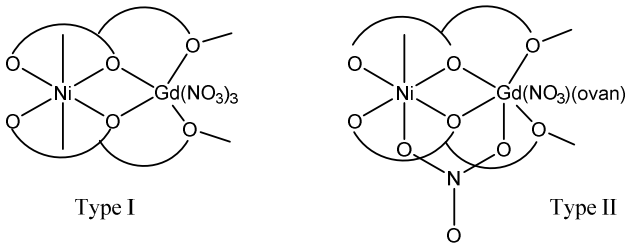

Scheme 1. Structures of type I and II for Ni^{II}-Gd^{III} complexes.

Results

In a previous paper, we showed that the reaction of Ni(o-van)$_2$(H$_2$O)$_2$ with lanthanide(III) ions allowed isolation of two types (I and II, respectively, see Scheme 1) of heterodinuclear Ni^{II}-Ln^{III} complexes. With lighter Ln^{III} ions, Ce^{III} in the present work or Pr^{III},[17] these complexes are prepared in good yields. The Ni^{II} and Ln^{III} ions are bridged by two deprotonated ortho-

View Article Online
DOI: 10.1039/C7DT04293K

vanillin ligands (o-van), the Ni^{II} coordination sphere being completed to six oxygen atoms by two water molecules in apical positions while the Ln^{III} ions are ten coordinate with their coordination sphere completed by three chelating nitrato anions. The second type of complexes was obtained with heavier Ln^{III} ions. In comparison to the first type of complex, a chelating nitrato ligand was replaced by an o-van ligand while a water molecule on the Ni^{II} ion was replaced by the oxygen atom of a bridging nitrato anion. These changes introduce a larger deformation of the equatorial plane and a decrease of the Ln^{III} coordination from ten to nine. At first, we reproduced this simple reaction in different conditions, allowing us to isolate several new complexes and, as such, to understand the Gd^{III} complexation with the $Ni(o\text{-}van)_2(H_2O)_2$ complex. Working with acetonitrile a type-I complex is isolated with an acetonitrile molecule replacing a water molecule (complex **5**). In acetone the reaction is more puzzling. Addition of isopropyl alcohol to an acetone solution resulting from the reaction of $Ni(o\text{-}van)_2(H_2O)_2$ with $Tb(NO_3)_3{\cdot}6H_2O$ yielded nice crystals corresponding to type-I complex **1** with two isopropyl alcohol molecules in place of the water ligands (complex **3**). These crystals are stable in their solution or in grease but in an open atmosphere they readily give powders analyzed as complex **4**, a water molecule replacing an isopropyl alcohol one. They can also be obtained by heating of the acetone/isopropyl alcohol solution. Eventually, the expected type-I Ni^{II}-Gd^{III} complex with two water molecules in the nickel(II) coordination sphere was obtained by diffusion of diethyl ether into an acetone solution, without heating of the filtered solution. Complex **1** is not as stable as expected since it can be transformed to type-II complex, as shown previously, but it can also yield a new type of tetranuclear complexes (type-III) after heating in acetone, methanol or ethanol. Only one of these tetranuclear complexes gave crystals by acetone diffusion into a methanol solution of the $Ni(o\text{-}van)_2(H_2O)_2$ and $Gd(NO_3)_3{\cdot}6H_2O$ reactants. This complex **7** does correspond to a tetranuclear Ni^{II}_2-Gd^{III}_2 entity with a defect-dicubane central core in which two nickel(II) ions are linked with methoxo and hydroxo bridges. Depending on the reaction conditions and according to the analytical results, the bridges can be modified, going from mixed hydroxo-methoxo bridges (complex **7**) to pure hydroxo (complexes **8** and **10**) or methoxo (complex **9**) ones. Infrared data are informative to differentiate these three different types of complexes. A look at the C=O stretching bands indicates that two bands are present in the 1624-1622 and 1611-1608 cm^{-1} areas for type-I complexes. Two bands appear again for the tetranuclear type-III complexes but the higher band is shown in the 1643-1635 cm^{-1} zone. For type-II dinuclear complexes three bands can be seen, the highest being in the 1629-1628 cm^{-1} zone.

Structure determinations

The complexes **1**, **2**, **3**, **5** crystallize in the monoclinic space group $P2_1/c$ with $Z = 4$. Since the structural determinations confirm several common features, we only report Figure 1 for complex **1** and Figure 2 for complex **5**, the other Figures appearing in the SI as Figures S1 (complex **2**) and S2 (complex **3**), with selected bonds and angles given in the corresponding captions. Two o-van ligands chelate the Ni^{II} and Ln^{III} ions, yielding central and practically planar NiO_2Ln cores, with the deprotonated phenoxo functions bridging the metal ions. The three nitrato anions are chelated to the Ln^{III} ion, which are ten-coordinate, surrounded by oxygen atoms coming from deprotonated phenoxo functions (2) and methoxy groups (2) of the two o-van ligands and from the nitrato anions (6). The Ni^{II} ions are six-coordinate to the phenoxo (2) and aldehyde (2) o-van oxygen atoms and to two donor atoms in axial position. These donor atoms belong to water molecules in complexes **1** and **2**, isopropyl alcohol molecules in complex **3**, and to water and CH_3CN molecules in complex **5**. These axial Ni-O or Ni-N bonds are slightly larger (2.058(2)-2.068(2) Å) than the Ni-O equatorial ones (2.001(2)-2.029(2) Å). These complexes correspond to the type-I complexes.

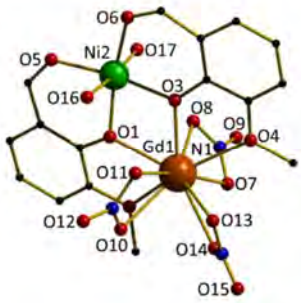

Figure 1. The molecular structure of **1** with atom numbering. Hydrogen atoms are omitted for clarity. Selected bond lengths and angles: Ni-O1 2.007(2), Ni-O2 2.001(2), Ni-O5 2.008(2), Ni-O6 2.015(2), Ni-O16 2.067(2), Ni-O17 2.068(2), Gd-O1 2.340(2), Gd-O2 2.345(2), Gd-O3 2.345(2), Gd-O4 2.532(2), Gd-O7 2.499(2), Gd-O8 2.522(2), Gd-O10 2.540(2), Gd-O11 2.536(2), Gd-O13 2.552(2), Gd-O14 2.491(2) Å, O1 Ni O2 78.79(8), O1 Gd O2 65.76(7), Ni O1 Gd 107.72(9), Ni O3 Gd 107.72(9)°.

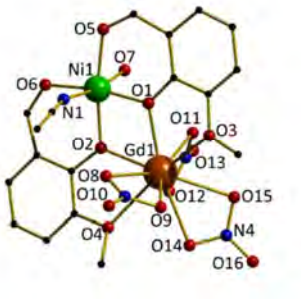

Figure 2. The molecular structure of **5** with atom numbering. Hydrogen atoms are omitted for clarity. Selected bond lengths and angles: Ni-O1 2.003(2), Ni-O2 2.014(2), Ni-O5 2.028(2), Ni-O6 2.029(2), Ni-O7 2.058(2), Ni-N1 2.068(2), Gd-O1 2.368(2), Gd-O2 2.335(2), Gd-O3 2.563(2), Gd-O4 2.560(2), Gd-O8 2.483(2), Gd-O9 2.558(2), Gd-O11 2.476(2), Gd-O12 2.455(2), Gd-O14 2.543(2), Gd-O15 2.560(2) Å, O1 Ni O2 79.59(7), O1 Gd O2 66.29(6), Ni O1 Gd 106.59(7), Ni O2 Gd 107.48(7)°.

The complex $[Ni(o\text{-}van)_2(\mu\text{-}NO_3)(H_2O)Tb(o\text{-}van)(NO_3)]H_2O$ **6** is again a heterodinuclear Ni^{II}-Tb^{III} complex, isomorphous with

View Article Online
DOI: 10.1039/C7DT04293K

the previously described Ni^{II}-Y^{III} and Ni^{II}-Gd^{III} equivalents.[17] In comparison with the complexes **1**, **2**, **3** described above, there are three main structural differences in these type-II complexes. Instead of three chelating nitrato anions, the Tb^{III} coordination sphere involves only one chelating nitrato anion, the second one insuring a supplementary bridge between the Ni^{II} and Tb^{III} ions while the third one is replaced by a chelating deprotonated o-van ligand, the Tb^{III} ion becoming nine-coordinate. The Ni^{II} ion remains six-coordinate but a solvent molecule is replaced by the oxygen atom of the bridging nitrato anion. Eventually the two o-van ligands defining the nickel(II) equatorial plane depart from planarity, as depicted in Figure 3.

Complexes **7**, **8**, **9**, **10** correspond to a new type of Ni^{II}-Ln^{III} complexes. Complex **7**, formulated $[Gd(o\text{-}van)_2(NO_3)_2Ni(OH)(OMe)Ni(o\text{-}van)_2Gd(NO_3)_2]CH_3COCH_3$, is a centrosymmetric tetranuclear Ni^{II}_2-Gd^{III}_2 complex molecule with a defect-dicubane central core, as shown in Figure 4. Two nickel(II) ions and the two bridging groups (hydroxo and methoxo) that make a double bridge between the Ni^{II} ions occupy the vertices of the common face of the defect-dicubane structure. Note that the hydroxo anion is hydrogen-bridged to an acetone molecule. Each bridging group is also linked to a gadolinium(III) ion, so that it behaves as a μ_3-OR (R = H or CH_3) ligand. The four metal ions are involved in a plane in which the Ni^{II} ions occupy the central position. If each Ni^{II} ion is linked to the three other ions, there is no direct bridge in between the Gd^{III} ions, which are bridged only to the Ni^{II} ions. Surprisingly, the Ni^{II} and Gd^{III} metal ions are coordinated in the same way to two deprotonated o-van ligands, by the aldehyde and phenoxo oxygen atoms of a ligand and the phenoxo and methoxy oxygen atoms of the second ligand, which define six and five-membered rings around the metal centres. The phenoxo oxygen atoms are in a *trans* position around the Ni^{II} ion when they are in a *cis* position around the Gd^{III} ion. This set of o-van and bridging ligands yield six-coordinate Ni^{II} ions and five-coordinate Gd^{III} ions, the Gd^{III} coordination sphere being completed to nine by two supplementary chelating nitrato anions. The nickel environment can be considered as a distorted octahedron with a Λ configuration for one Ni^{II} ion and a Δ configuration for the other one, in agreement with the centrosymmetric space group found for these complexes. The Ni-O bonds are comprised between 1.991(5) to 2.043(5) Å, except for the Ni-O(methoxy) bond that is larger, 2.145(6) Å. As usual, the Gd-O bond lengths depend on the nature of the oxygen atoms, varying from 2.319(5) to 2.492(6) Å, the Gd-O (methoxy) bond being larger (2.622(6) Å). The OH-Ni-OH and Ni-OH-Ni angles deviate from 90°, with values of 84.6(2) and 95.4(2). There are intramolecular hydrogen bonds involving the non-coordinated acetone molecules and the hydroxo groups.

The structural determination demonstrates that the o-van ligands, which are roughly in the same plane in the starting nickel complex and in the dinuclear Ni^{II}-Ln^{III} entities, become practically perpendicular in the Ni^{II}_2-Gd^{III}_2 complex, which induces a change in the Ni^{II} and Gd^{III} coordination spheres. This new arrangement implies breaking at least one Ni-O and one Gd-O bonds. Since $Gd(NO_3)_3$ entities are non-electrolytes in acetone while they behave as 2/1 electrolytes in methanol,[37] and since these ionic species are acidic in protic solvents,[38] we understand the breaking of the bonds and the replacement of a nitrato ligand by an hydroxo one.

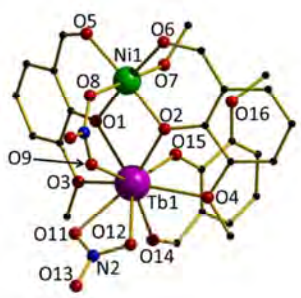

Figure 3. The molecular structure of **6** with atom numbering. Hydrogen atoms are omitted for clarity. Selected bond lengths and angles: Ni-O1 2.004(2), Ni-O2 1.990(3), Ni-O5 2.017(3), Ni-O6 2.031(3), Ni-O7 2.071(3), Ni-O8 2.073(4), Tb-O1 2.368(3), Tb-O2 2.314(3), Tb-O3 2.623(3), Tb-O4 2.565(3), Tb-O9 2.545(3), Tb-O11 2.447(3), Tb-O12 2.467(3), Tb-O14 2.344(3), Tb-O15 2.267(3), Ni...Tb 3.3476(6) Å, O1 Ni O2 84.92(11), O1 Gd O2 71.43(10), Ni O1 Gd 101.70(12), Ni O2 Gd 101.86(11)°.

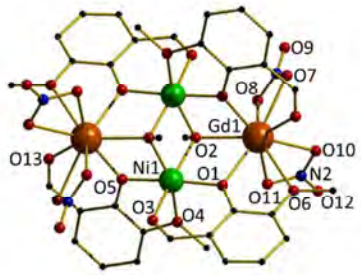

Figure 4. The molecular structure of **7** with atom numbering. Hydrogen atoms are omitted for clarity. Selected bond lengths and angles: Ni-O1 1.991(5), Ni-O2 2.042(4), Ni-O2' 2.041(4), Ni-O3 2.043(5), Ni-O4 2.145(6), Ni-O5 2.013(5), Gd-O1 2.369(5), Gd-O2 2.383(4), Gd-O5' 2.319(5), Gd-O6 2.622(6), Gd-O7 2.489(6), Gd-O8 2.467(7), Gd-O10 2.492(6), Gd-O11 2.463(6), Gd-O13 2.391(7), Gd...Ni 3.4821(9), Gd'...Ni 3.4146(9) Å, O1 Ni O2' 102.9(2), O2 Ni O2' 84.28(18), Ni O2 Ni' 95.7(2), Ni O2' Gd' 100.8(2), Ni O2 Gd 103.5(2), Ni O5' Gd' 103.8(2)°.

Magnetic properties

Figure 5 shows the susceptibility, as the $\chi_M T$ product, for complexes **1**, **4**, **5**, **7**, **8** and **9**. For complex **4**, $\chi_M T$ is equal to 9.43 $cm^3mol^{-1}K$ at 300 K, slightly increasing to 9.69 $cm^3mol^{-1}K$ at 100 K and then sharp increasing on further lowering *T* down to 5 K where it is equal to 12.30 $cm^3mol^{-1}K$. A slight decrease to 11.73 $cm^3mol^{-1}K$ is finally observed between 5 and 2 K. The $\chi_M T$ value at room temperature corresponds to the expected value of 9.5 $cm^3mol^{-1}K$ for one isolated Ni^{II} and one Gd^{III} ions, and g_{Ni} = 2.05, g_{Gd} = 2.

View Article Online
DOI: 10.1039/C7DT04293K

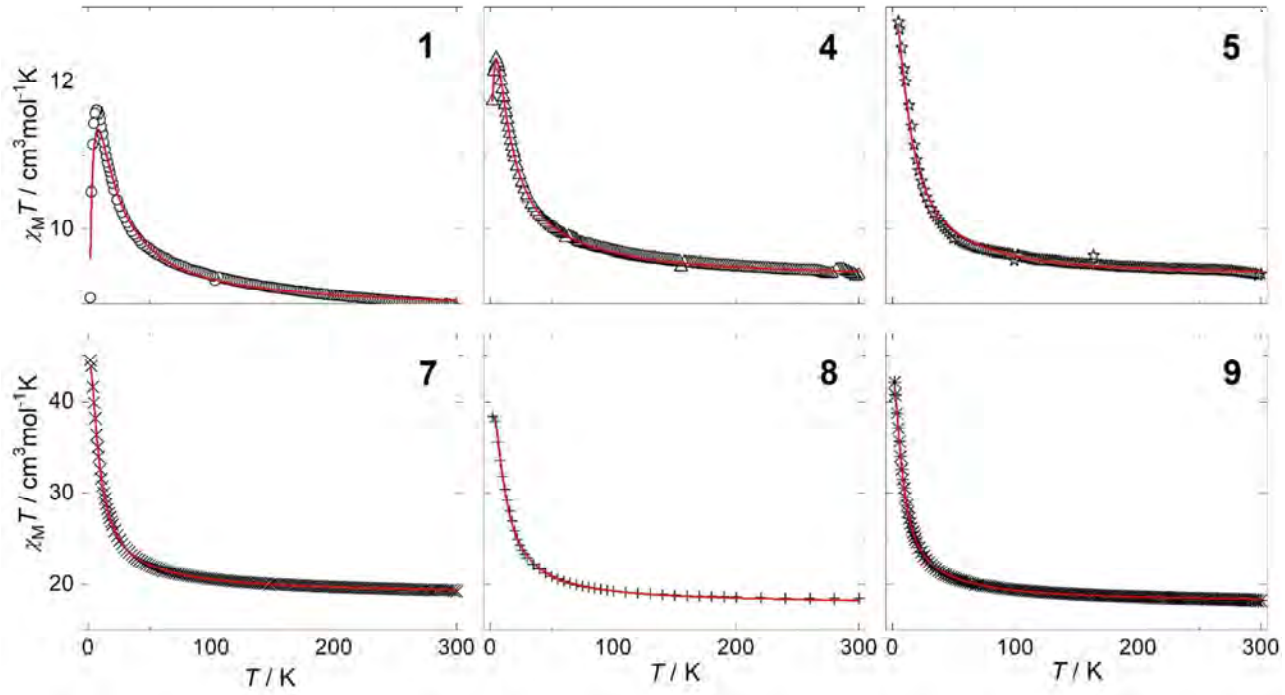

Figure 5. Temperature-dependence of the $\chi_M T$ product for complexes **1**, **4**, **5**, **7**, **8** and **9,** collected for the applied external field of 0.1 T. Solid red line corresponds to the best fits (see text).

The experimental data indicate the occurrence of an overall ferromagnetic interaction in complex **4**. The magnetic susceptibility has been computed by exact calculation of the energy levels, through diagonalization of the full energy-matrix, associated with the full spin-Hamiltonian:

$$\hat{H} = -J_{NiGd}\,\hat{s}_{Ni}\cdot\hat{s}_{Gd} + D_{Ni}s_z^2 + g_{Ni}\mu_B H s_{Ni} + g_{Gd}\mu_B H s_{Gd},$$

where the first term accounts for the magnetic exchange between the Ni^{II} and Gd^{III} ions, D_{Ni} is the uniaxial anisotropy parameter for the Ni^{II} ion, s_z is the z component of the $\hat{s}_{Ni}$ vector, and the last two terms correspond to the Zeeman interaction. An additional coupling parameter, zJ, has also been introduced to take into account the intermolecular interactions within the frame of the molecular field approximation. The best fit yields J_{NiGd} = 2.48 cm^{-1}, D_{Ni} = 4.7 cm^{-1}, g_{Ni} = 2.05, zJ = 0.005 cm^{-1}, with a r factor equal to 1.0 $\times$ 10^{-5}, $r = \Sigma[(\chi_M T)^{obs} - (\chi_M T)^{calc}]^2 / [\Sigma (\chi_M T)^{obs}]^2$. In the absence of the weak zJ term, the fit at low temperature is not good and the D_{Ni} term is overestimated. Conversely, the introduction of the zJ term does increase the quality of the fit and furnishes a D_{Ni} term in agreement with previous values.[39] In order to check the validity of these results, the Magpack program[22,23] has been used to fit the experimental magnetization curve at low temperature. As we cannot include the zJ term in that program, the calculated magnetization is slightly larger than the experimental data in the 0.5-2 T domain. Nevertheless, this result confirms the ferromagnetic Ni^{II}-Gd^{III} interaction and the presence of a zero-field splitting (ZFS) term for the Ni^{II} ion (Figure S3).

The same Hamiltonian is also used to model the magnetic properties of the Ni^{II}-Gd^{III} dimers **1** and **5**. The best fits of the susceptibilities and the isothermal magnetizations (Figures S4 and S5) give: J_{NiGd} = 2.77 cm^{-1}, D_{Ni} = 2.8 cm^{-1}, g_{Ni} = 2.03, zJ = −0.017 cm^{-1} with a r factor equal to 2.0 $\times$ 10^{-5} for **1** and J_{NiGd} = 2.31 cm^{-1}, D_{Ni} = 0.7 cm^{-1}, g_{Ni} = 2.04 with a r factor equal to 2.0 $\times$ 10^{-5} for **5**.

For complex **7**, $\chi_M T$ is practically constant from 300 K (19.19 cm^{3}mol^{-1}K) to 100 K (20.60 cm^{3}mol^{-1}K), while it increases sharply below 50 K till 44.50 cm^{3}mol^{-1}K at 2 K. The value at room temperature is larger than the expected for two Ni^{II} and two Gd^{III} ions without interaction and with $g_{Ni} = g_{Gd}$ = 2 (17.75 cm^{3}mol^{-1}K). This difference comes from an underestimation of the nickel(II) $\chi_M T$ contribution, the g_{Ni} factor being larger than 2. On the contrary, the $\chi_M T$ value at 2 K is not far from what is expected for a complex with active ferromagnetic interactions (45 cm^{3}mol^{-1}K). From the structural determination of complex **7**, it is clear that each Ni^{II} ion interacts with the other Ni^{II} ion and also with the two Gd^{III} ions, while the Gd^{III} ions do not interact between themselves. Therefore, the spin-Hamiltonian used to fit these susceptibility data is

$$\hat{H} = -J_{NiNi}\,\hat{s}_{Ni1}\cdot\hat{s}_{Ni2} - J_{NiGd}\,(\hat{s}_{Ni1}\cdot\hat{s}_{Gd1} + \hat{s}_{Ni1}\cdot\hat{s}_{Gd2} + \hat{s}_{Ni2}\cdot\hat{s}_{Gd1} + \hat{s}_{Ni2}\cdot\hat{s}_{Gd2}) + 2D_{Ni}s_z^2 + g_{Ni}\mu_B H s_{Ni1} + g_{Ni}\mu_B H s_{Ni2} + g_{Gd}\mu_B H s_{Gd1} + g_{Gd}\mu_B H s_{Gd2}.$$

The best fit yields J_{NiNi} = 43.8 cm^{-1}, J_{NiGd} = 1.21 cm^{-1}, D_{Ni} = 5.8 cm^{-1}, g_{Ni} = 2.06, with a r factor equal to 1.0 $\times$ 10^{-5} for **7**. The

View Article Online
DOI: 10.1039/C7DT04293K

experimental magnetization curves for T = 2-10 K (Figure S6) are nicely fitted with these values introduced in the Magpack program, hence confirming that only ferromagnetic interactions are present in the tetranuclear dicubane complex.

Complexes **8** and **9** are again tetranuclear dicubane defect complexes with respectively di-hydroxo or di-methoxo bridges instead of the mixed hydroxo-methoxo bridges present in complex **7**. The fits of the $\chi_M T$ vs. T curves give: J_{NiNi} = 25.0 cm^{-1}, J_{NiGd} = 1.40 cm^{-1}, g_{Ni} = 2.00, D_{Ni} = 5.5 cm^{-1}, r = 2.0 × 10^{-5} for **8**, and J_{NiNi} = 33.8 cm^{-1}, J_{NiGd} = 1.12 cm^{-1}, g_{Ni} = 2.01, D_{Ni} = 5.5 cm^{-1}, r = 1.0 × 10^{-5} for **9**. A very weak zJ term (zJ = −0.002 cm^{-1}) is introduced for complex **8**. The magnetization values of 17.6 and 17.9 $N\mu_B$ at 2 K and 5 T (see Figures S7 and S8) confirm the S = 9 ground state of these two complexes **8** and **9**.

The value of J_{NiGd} is correlated to the hinge angle, the dihedral angle between the O-Ni-O and O-Gd-O planes of the central Ni(O_2)Gd core of the molecule, and the Ni-O-Gd bridging angles. In **1**, **5** and **7**, the hinge angles are very similar, varying from 1 to 3°. The bridging Ni-O-Gd angles are equal to 108° for **1** and 107° for **5**, which is in agreement with similar J_{NiGd} values for **1** and **5**, i.e., 2.77 and 2.31 cm^{-1}, respectively. Differently, the bridging angle decreases to 102° for complex **7** and, correspondingly, J_{NiGd} decreases to 1.21 cm^{-1}. These values do agree with previous published data, the largest J_{NiGd} values (2-3 cm^{-1}) corresponding to bridging angles equal to 109-110°, while angles of ca. 100° yield J_{NiGd} values of ca. 1 cm^{-1}.[40]

In order to check the ferromagnetic Ni^{II}-Ni^{II} interaction for the tetranuclear dicubane complexes, the Gd^{III} ion is replaced in **10** by a diamagnetic Y^{III} ion, so that the Ni^{II}-Ni^{II} interaction is the only magnetic active parameter. The $\chi_M T$ for **10** (Figure S9) varies from 3.25 cm^{3}mol^{-1}K at 300 K to 3.12 cm^{3}mol^{-1}K at 140 K, passing through a maximum of 3.68 cm^{3}mol^{-1}K at 15 K, and it decreases to 2.99 cm^{3}mol^{-1}K at 2 K. This behavior confirms the presence of a ferromagnetic Ni^{II}-Ni^{II} interaction that we quantify by the use of the spin-Hamiltonian

$$\hat{H} = -J_{NiNi}\,\hat{s}_{Ni1}\cdot\hat{s}_{Ni2} + D_{Ni}s_z^{\,2} + g_{Ni}\mu_B H s_{Ni1} + g_{Ni}\mu_B H s_{Ni2},$$

obtaining J_{NiNi} = 25.0 cm^{-1}, g_{Ni} = 2.22, D_{Ni} = 5.4 cm^{-1} and r = 1.3 × 10^{-5} for **10**. The 4 $N\mu_B$ magnetization value confirms the S = 2 ground state at 2 K (Figure S10). It should be noted that a temperature independent paramagnetism term (TIP) is needed to fit the high-temperature domain of the $\chi_M T$ curve.

Heat capacity properties

Measurements of the heat capacity, C/R, where R is the gas constant, are shown in Figure 6 for complexes **1**, **5** and **7.** The non-magnetic, lattice heat capacity, C_{latt}, is the dominant contribution above 5-10 K for each complex. The fit to the Debye model (dashed lines in Fig. 6) gives the Debye temperature Θ_D = 54.5 K for **1**, 61.4 K for **5** and 39.5 K for **7**, which is consistent with typical values reported for molecular nanomagnets.[41] Below 5 K, the lattice contribution rapidly vanishes and field-dependent Schottky anomalies arise from the splitting of the spin levels. The dependence on the applied field of the magnetic contribution to the heat capacity, i.e., $C_m = C - C_{latt}$, is reasonably well reproduced (solid lines in Fig. 6) by using the same models and sets of parameters obtained from fitting the magnetic data. Discrepancies become evident on lowering the applied field and temperature, i.e., when intermolecular interactions become relevant, since they are not taken into account in the spin-Hamiltonian used to model the magnetic data.

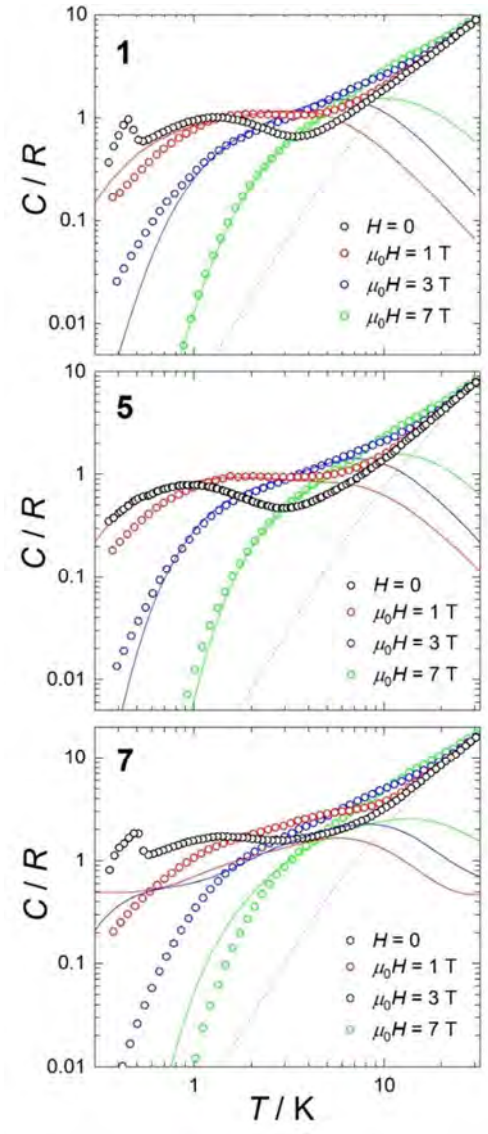

Figure 6. Temperature-dependence of the molar heat capacity, C/R, where R is the gas constant, for complexes **1**, **5** and **7** (from top to bottom, respectively), collected for several applied magnetic fields, as labelled. Solid lines are the calculated magnetic contributions by making use of the model and parameters obtained from fitting the magnetic data. Dashed lines are the calculated lattice contributions.

For **1** and **7**, the zero-field (H = 0) heat capacity shows a sharp peak, which is superimposed to the low-T tail of the Schottky anomaly and centered at T = 0.49 K and 0.45 K, respectively. For both complexes, the peak is promptly and fully removed by applying the magnetic field, denoting that it has to be associated with a magnetic phase transition. Differently, no marked feature characterizes the zero-field heat capacity of **5**

View Article Online
DOI: 10.1039/C7DT04293K

other than the Schottky anomaly. Nonetheless, a tiny yet discernible anomaly can be seen to occur at ca. 0.5 K, which is probably ascribed to the onset of a magnetic phase transition. The almost full suppression of the peak in **5** is likely the result of the presence of acetonitrile molecules that, by preventing the formation of hydrogen bonds, strongly restrain the intermolecular interactions.

Intermolecular correlations start to develop below ca. 2-3 K, concomitantly with the stabilization of the highest spin state per molecule. As can be seen in Fig. S11, the value of the zero-field molar entropy $S/R = \int C/(RT)\mathrm{d}T$ at these temperatures is consistent with full ferromagnetic intramolecular alignment, which corresponds to one Ni^{II} spin, s_{Ni}, and one Gd^{III} spin, s_{Gd}, per molecule, i.e., $\ln(2 \times S_{tot} + 1) = 2.3$, where $S_{tot} = s_{Gd} + s_{Ni} = 9/2$, for **1** and **5**, and to two Ni^{II} spins and two Gd^{III} spins per molecule, i.e., $\ln(2 \times S_{tot} + 1) = 2.9$, where $S_{tot} = 2 \times s_{Ni} + 2 \times s_{Gd} = 9$, for **7**. Note that the lattice contribution to the entropy is negligible at these temperatures (Fig. S11). As the temperature is increased above these values, the entropy content associated with the ferromagnetic intramolecular ordering is gradually removed, as seen by the continuously increasing $S(T)$ curves in Figure S11. The maximum magnetic entropy value per mole is calculated as $S_m^{max}/R = \ln(2 \times s_{Gd} + 1) + \ln(2 \times s_{Ni} + 1) = 3.2$ for **1** and **5**, and to $2 \times \ln(2 \times s_{Gd} + 1) + 2 \times \ln(2 \times s_{Ni} + 1) = 6.4$ for **7**. This value is not reached experimentally since the determination of the magnetic entropy $S_m(T)$ becomes too uncertain above the temperature of ca. 10 K.

Discussion

We have already shown that the use of a compartmental Schiff base of the salen-type ligand involving o-vanillin is able to give an isostructural Ni^{II}-Ln^{III} series on going from lighter to heavier Ln^{III} ions.[42] More recently, we have demonstrated that replacement of the Schiff base by o-vanillin alone does not yield a simple heterodinuclear Ni^{II}-Ln^{III} series, complexes of different composition being isolated.[17] At that time, we could identify two types of complexes. With light Ln^{III} ions, the Ni^{II} ion is chelated in a cis conformation to two o-vanillin ligands by the aldehyde and phenoxo oxygen atoms, the Ln^{II} ion occupying the outer O_2O_2 coordination site implying the phenoxo and methoxy oxygen atoms. The Ln^{III} ion is ten-coordinate, the three chelating nitrato anions completing the Ln^{III} coordination sphere while the Ni^{II} ion is in an octahedral environment, with two axial water molecules (type-I complexes). Here, we show that the equivalent Ni^{II}-Gd^{III} complex **1** can be prepared, as confirmed by its structural determination, but it is isolated in low yield in comparison to the Ni^{II}-Ce^{III} equivalent **2**, i.e., 15 % against 75 %, respectively. Furthermore, while the Ni^{II}-Ce^{III} preparation is straightforward, the situation becomes more complex for Ni^{II}-Gd^{III}. This is why we had a special interest to that puzzling question. These type-I complexes are obtained in acetone (Ni^{II}-Ce^{III}) or a mixture of non-protic solvents (acetone-diethyl ether for Ni^{II}-Gd^{III} complex **1**). An acetone-acetonitrile mixture gives a similar complex in which a water molecule is replaced by a CH_3CN molecule (complex Ni^{II}-Gd^{III} **5**) while an acetone-isopropyl alcohol mixture allows isolation of a very unstable Ni^{II}-Tb^{III} complex **3** with two isopropyl molecules replacing the axial water ones. These crystals effloresce very quickly to give powders corresponding to the $[Ni(o\text{-}van)_2(iPrOH)(H_2O)Ln(NO_3)_3]$ formulation ($Ln^{III} = Gd^{III}$, Tb^{III}).

Use of protic solvents such as methanol followed by addition of isopropyl alcohol allows crystallization of the Ni^{II}-Tb^{III} complex **6** that corresponds to the previously characterized Ni^{II}-Y^{III} type-II complex. In this experimental process, part of the initial $Ni(o\text{-}van)_2(H_2O)_2$ complex is destroyed for a supplementary o-vanillin ligand replaces a nitrato anion, the Ni^{II} ion being still chelated to two o-vanillin ligands in a cis conformation (type-II complex). The same reaction in methanol alone furnishes green powders that do not correspond to the type-II complexes. The addition of acetone to the methanol solution yielded crystals that highlight a new type of complexes with a defect-dicubane structure, as observed for complex **7**. Therefore, the addition of gadolinium nitrate to $Ni(o\text{-}van)_2(H_2O)_2$ can yield three types of Ni^{II}-Ln^{III} complexes with different chemical formulas corresponding to heterodinuclear (Ni^{II}-Ln^{III}, type-I or II) or heteroteteranuclear (Ni^{II}_2-Ln^{III}_2, type-III). This confirms that the use of o-vanillin instead of a Schiff base ligand derived from o-vanillin gives a richer chemistry, which is much more complex and more difficult to master.

The use of the "SHAPE program" allows to quantify the deformation of the nickel coordination sphere from the ideal octahedron geometry with help of the continuous shape measure parameters S(Oh), S(Oh) being equal to 0 for a perfect octahedron. For complexes **1**, **2**, **3**, S(Oh) are respectively equal to 0.50, 0.31 and 0.40. The value slightly increases for complex **5** (S(Oh) = 0.81), where a nitrogen atom replaces an oxygen atom in axial position and becomes larger in complex **7** (S(Oh) = 1.31), the tetranuclear structure being more constrained. It is in the type-II complex **6** that the Ni^{II} ion is practically in a perfect octahedral environment (S(Oh) = 0.14), as observed in the previous work.[17]

A look at the magnetic properties does confirm that the dinuclear Ni^{II}-Gd^{III} complexes are characterized by very similar interaction parameters, J_{NiGd} varying from 2.31 to 2.77 cm^{-1}, with positive axial zero-field splitting D_{Ni} terms going from 0.7 to 4.7 cm^{-1}. We have shown in a previous work that an increase of D_{Ni} corresponds to an axial elongation of the Ni-O(N) bond lengths.[39] This study also showed that D_{Ni} for the type-II $[Ni(o\text{-}van)_2(\mu\text{-}NO_3)(H_2O)Y(o\text{-}van)(NO_3)]H_2O$ complex was negative,[39] which explains the synthesis and magnetic study of the equivalent $[Ni(o\text{-}van)_2(\mu\text{-}NO_3)(H_2O)Tb(o\text{-}van)(NO_3)]H_2O$ complex **6** in order to check if it behaves as a single-molecule magnet. Unfortunately, observation of a negative result highlights the complexity of the SMM problem, introduction of two anisotropic ions inducing not necessarily a positive effect on the SMM behavior. We previously showed that trinuclear Co^{II}-Gd^{III}-Co^{II} complexes in which anisotropy comes from the Co^{II} ions, behave as SMM.[43,44] A similar behavior could be expected in our tetranuclear Ni^{II}_2-Gd^{III}_2 complexes, Ni^{II} ions being anisotropic and the Ni^{II}-Ni^{II} and Ni^{II}-Gd^{III} magnetic

View Article Online
DOI: 10.1039/C7DT04293K

interactions being ferromagnetic. However, ac measurements gave again a negative response.

Finally, we have studied the magnetocaloric properties for some representative compounds, namely **1**, **5** and **7**, that are interesting for magnetic refrigeration application, mainly due to their gadolinium content. A further reason of interest in terms of this application is that complexes **1**, **5** and **7** are characterized by relatively small molecular masses. More specifically, the ratio of the metal ion mass compared to the molecular mass is significantly large, in addition to being very similar for each compound, since it is equal to 29.2 %, 28.3 % and 31.1 %, for **1**, **5** and **7**, respectively. Note that a large magnetic density implies a correspondingly large content of magnetic entropy, which can ultimately favor a large magnetocaloric effect. From our experiments, in particular from the entropy curves $S(T, H)$, plotted in Figure S11, we estimate the magnetic entropy change $-\Delta S_m(T, \Delta H) = S(T, H_i) - S(T, H_f)$ and the adiabatic temperature change $\Delta T_{ad}(T_f, \Delta H) = T_i(S, H_i) - T_f(S, H_f)$, that follow the change of the applied field $\Delta H = H_i - H_f$. Note that the lattice entropy is irrelevant for the estimation of ΔS_m, because it is non-magnetic and thus it cancels out.

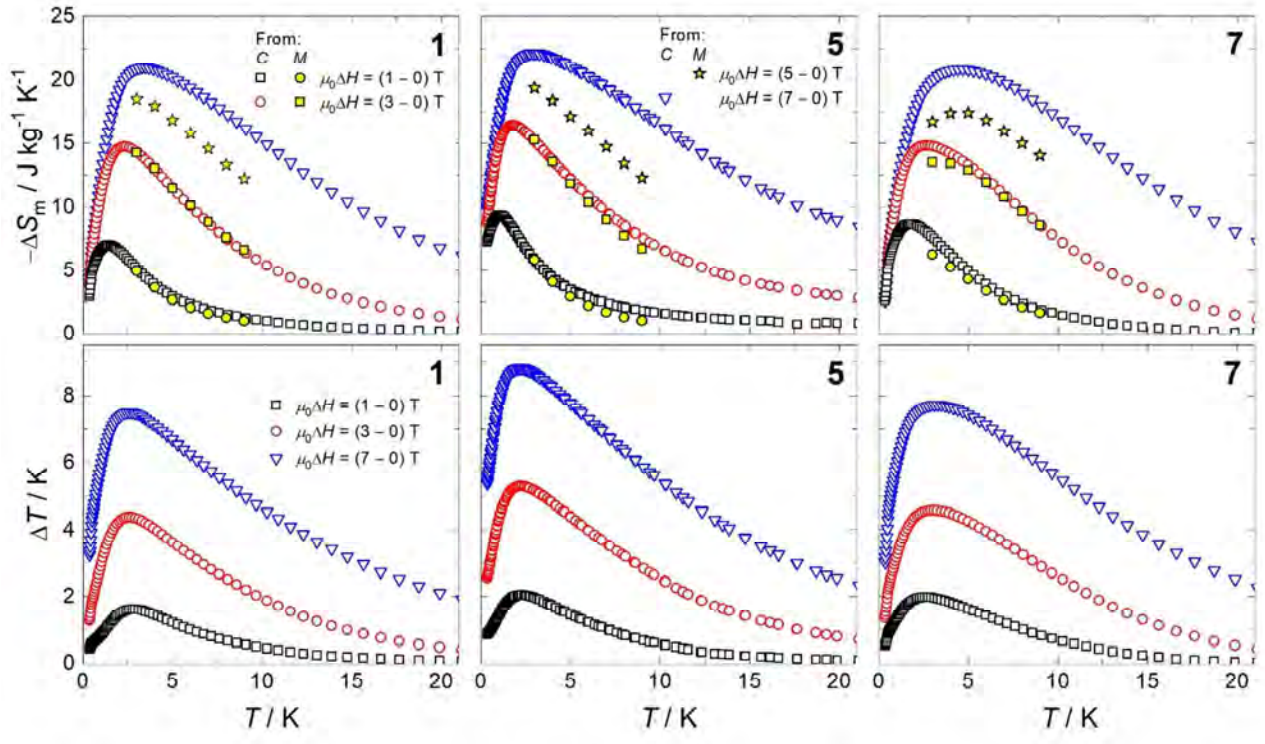

Figure 7. Top, from left to right (for complexes **1**, **5** and **7**, respectively): Temperature-dependence of the magnetic entropy change for the indicated applied field changes, as obtained from heat capacity and magnetization data (see text). Bottom, from left to right (for complexes **1**, **5** and **7**, respectively): Temperature-dependence of the adiabatic temperature change for the indicated applied field changes, as obtained from heat capacity data (see text).

The resulting curves for **1**, **5** and **7** are plotted in Figure 7 for $\mu_0\Delta H$ = 1, 3 and 7 T, where H_f = 0. The magnetic entropy change is calculated additionally for $\mu_0\Delta H$ = 1, 3 and 5 T by applying the Maxwell equation $-\Delta S_m(T, \Delta H) = \int(\partial M/\partial T)_H dH$ to the magnetization M data (see Figures S4, S5 and S6). The good agreement between the two sets of $\Delta S_m(T, \Delta H)$ data, obtained independently from $C(T, H)$ and $M(T, H)$, confirms the correctness of the procedures employed. The overall trend of the MCE shows maxima in $-\Delta S_m(T, \Delta H)$ and $\Delta T_{ad}(T_f, \Delta H)$ at relatively low temperatures, mainly driven by the weak strength of the underlying magnetic interactions. In particular, the maximum values reached by $-\Delta S_m(T, \Delta H)$ for $\mu_0\Delta H$ = 7 T are rather similar for each compound and corresponds to 21.0 J kg^{-1}K^{-1} at T = 3.5 K for **1**, 22.1 J kg^{-1}K^{-1} at T = 2.9 K for **5**, and 20.9 J kg^{-1}K^{-1} at T = 4.7 K for **7**. The adiabatic temperature change $\Delta T_{ad}(T_f, \Delta H)$ behaves in a similar manner for the three compounds, reaching the maximum values of 7.5 K at T_f = 2.4 K for **1**, 8.8 K at T_f = 2.2 K for **5**, and 7.7 K at T_f = 2.9 K for **7**, all for $\mu_0\Delta H$ = 7 T. The overall slightly larger MCE for **5** can be understood by a comparison with **1**. Both complexes are very similar to one another, in terms of the magnetic density and strength of the exchange coupling J_{NiGd}, regardless of the intermolecular interactions that are too weak to play any significant role above 1 K and/or 1 T. The one and only relevant difference is the single-ion anisotropy D_{Ni}, which amounts to 2.8 cm^{-1} for **1** and 0.7 cm^{-1} for **5**, as obtained from fitting the magnetization data.

It should be emphasized that, by limiting the spin degrees of freedom, the magnetic anisotropy hinders the MCE, that is, it lowers the $-\Delta S_m(T, \Delta H)$ and $\Delta T_{ad}(T, \Delta H)$ curves, while broadening and shifting them towards higher T, the more so the larger the anisotropy.[19] Therefore, the behavior to be

View Article Online
DOI: 10.1039/C7DT04293K

expected is nicely consistent with the observations. The magnetocaloric properties of several other Ni^{II}-Gd^{III} molecular complexes have been reported so far. The here-investigated MCE for **1**, **5** and **7** is larger than in most cases,[45] with the exception of those characterized by a relatively higher Gd^{III} nuclearity with respect to Ni^{II}.[46]

Conclusions

This paper demonstrates that the use of a simple ligand such as o-vanillin allows the preparation of heterodinuclear Ni^{II}-Ln^{III} complexes. In comparison of Ni^{II}-Ln^{III} complexes made with Schiff bases, two o-van ligands are needed instead of the unique Schiff base ligand. This difference introduces a supplementary degree of freedom from the synthetic point of view, which increases the synthetic possibilities. Furthermore, the Lewis acidity increase of the Ln^{III} ions in protic solvents, on going from lighter to heavier Ln^{III} ions, favors the formation of type-II and type-III complexes, at the expense of type-I complexes. Nevertheless, this later effect can be moderated by the use of acetonitrile. Only ferromagnetic intramolecular interactions are active above $T \approx 2$ K in the entire set of dinuclear and tetranuclear Ni^{II}-Gd^{III} complexes, the Ni^{II}-Ni^{II} interactions being larger than the Ni^{II}-Gd^{III} ones. Below ca. 2 K, intermolecular correlations start to develop, ultimately leading to a magnetically ordered state at $T = 0.49$ K and, similarly, at ca. 0.5 K for the dinuclear Ni^{II}-Gd^{III} complexes **1** and **5**, respectively, and at $T = 0.45$ K for the tetranuclear Ni^{II}-Gd^{III} complex **7**. The magnetocaloric effect of **1**, **5** and **7**, determined from magnetization and heat capacity experiments, is maximum in the range of ca. $1\ K \leq T \leq 6$ K. Besides, comparatively with studies for other Ni^{II}-Gd^{III} complexes, the effect is relatively large, the more so the lower is the magnetic anisotropy of the Ni^{II} ions.

Acknowledgements

This work has been supported by Spanish MINECO through grant MAT2015-68204-R (to M.E. and G.L.) and a postdoctoral contract (to G. L.), by CNRS and MAGMANet (Grant NMP3-CT-2005-515767).

Notes and references

1 C. Benelli, D. Gatteschi, *Chem. Rev.*, 2002**, *102,*** 2369.
2 M. Sakamoto, K. Manseki, H. Okawa, *Coord. Chem. Rev.*, 2001, ***219-221***, 379.
3 (a) M. Andruh, J. P. Costes, C. Diaz, S. Gao, *Inorg. Chem.*, 2009, **48**, 3342. (b) M. Andruh, *Dalton Trans.*, 2015, **44**, 16633.
4 R. Sessoli, A. K. Powell, *Coord. Chem. Rev.*, 2009, **253**, 2328.
5 Y. G. Huang, F. L. Jiang, M. C. Hong, *Coord. Chem. Rev.*, 2009, **253**, 2814.
6 H. L. C. Feltham, S. Brooker, *Coord. Chem. Rev.*, 2014, **276**, 1.
7 A. J. McKinnon, T. N. Waters, D. Hall, *J. Chem. Soc.,* 1964, **0**, 3290.
8 J. M. Stewart, E. C. Lingafelter, J. D. Breazeale, *Acta Cryst.*, 1964, **17**, 1481.
9 H. Guo, G. Zhao, *Asian J. Chem.*, 2008, **20**, 2781.
10 J. P. Costes, F. Dahan, F. Nicodème, *Inorg. Chem.*, 2001, **40**, 5285.
11 J. Tang, I. Hewitt, N. T. Madhu, G. Chastanet, W. Wernsdorfer, C. E. Anson, C. Benelli, R. Sessoli, A. K. Powell, *Angew. Chem. Int. Ed.*, 2006, **45**, 1729.
12 J. Luzón, K. Bernot, I. J. Hewitt, C. E. Anson, A. K. Powell, R. Sessoli, *Phys. Rev. Lett.*, 2008, **100**, 247205.
13 L. F. Chibotaru, L. Ungur, A. Soncini, *Angew. Chem. Int. Ed.*, 2008, **47**, 4126.
14 J. P. Costes, F. Dahan, A. Dupuis, J. P. Laurent, *Inorg. Chem.*, 1997, **36**, 3429.
15 T. Kajiwara, M. Nakano, S. Takaishi, M. Yamashita, *Inorg. Chem.*, 2008, **47**, 8604.
16 J. P. Costes, F. Dahan, A. Dupuis, J. P. Laurent, *C. R. Acad. Sci. Paris*, IIc, 1998, 417.
17 J. P. Costes, L. Vendier, *Eur. J. Inorg. Chem.*, 2010, 2768.
18 J. P. Costes, L. Vendier, W. Wernsdorfer, *Dalton Trans.*, 2011, **40**, 1700.
19 M. Evangelisti, E. K Brechin, *Dalton Trans.*, 2010, **39**, 4672.
20 (a) For a recent overview, see, for example, J. W. Sharples, D. Collison, *Polyhedron*, 2013, **54**, 91, and references therein. (b) J. W. Sharples, D. Collison, E. J. L. McInnes, J. Schnack, E. Palacios, M. Evangelisti, *Nat. Commun.*, 2014, **5**, 5321.
21 P. Pascal, *Ann. Chim. Phys.*, 1910, **19**, 5.
22 A. K. Boudalis, J. M. Clemente-Juan, F. Dahan, J. P. Tuchagues, *Inorg. Chem*, 2004, **43**, 1574.
23 (a) J. J. Borrás-Almenar, J. M. Clemente-Juan, E. Coronado, B. S. Tsukerblat, *Inorg. Chem.*, 1999, **38**, 6081. (b) J. J. Borrás-Almenar, J. M. Clemente-Juan, E. Coronado, B. S. Tsukerblat, *J. Comput. Chem.*, 2001, **22**, 985.
24 F. James, M. Roos, "*MINUIT Program*, a System for Function Minimization and Analysis of the Parameters Errors and Correlations", *Comput. Phys. Commun.*, 1975, **10**, 343.
25 Agilent Technologies (2011). Agilent Technologies UK Ltd., Oxford, UK, Xcalibur CCD system, CrysAlisPro Software system, Version 1.171.35.19.
26 *CrysAlis CCD*, *CrysAlis RED* and associated programs: Oxford Diffraction (2006). *Program name(s)*. Oxford Diffraction Ltd, Abingdon, England.
27 *STOE: IPDS Manual*, version 2.75; Stoe & Cie, Darmstadt, Germany, 1996.
28 *SAINT* Bruker (2007). Bruker AXS Inc., Madison, Wisconsin, USA.
29 C. K. Fair, *MolEN*, *Structure Solution Procedures*; Enraf-Nonius: Delft, Holland, 1990.
30 A. C. T. North, D. C. Phillips, F. S. Mathews, *Acta Crystallogr., Sect. A*, 1968, **A24**, 351.
31 SHELX97 [Includes SHELXS97, SHELXL97, CIFTAB] - Programs for Crystal Structure Analysis (Release 97-2). G. M. Sheldrick, Institüt für Anorganische Chemie der Universität, Tammanstrasse 4, D-3400 Göttingen, Germany, 1998.
32 SIR92 - A program for crystal structure solution. A. Altomare, G. Cascarano, C. Giacovazzo, A. Guagliardi, *J. Appl. Crystallogr.*, 1993, **26**, 343.
33 WINGX - 1.63 Integrated System of Windows Programs for the Solution, Refinement and Analysis of Single Crystal X-Ray Diffraction Data. L. Farrugia, *J. Appl. Crystallogr.*, 1999, **32**, 837.
34 International tables for X-Ray crystallography, Vol IV, Kynoch press, Birmingham, England, 1974.
35 L. Zsolnai, H. Pritzkow, G. Huttner, *ZORTEP*. Ortep for PC, Program for Molecular Graphics, University of Heidelberg, Heidelberg, Germany, 1996.
36 ORTEP3 for Windows - L. J. Farrugia, *J. Appl. Crystallogr.*, 1997, **30**, 565.
37 J. P. Costes, J. Garcia-Tojal, J. P. Tuchagues, L. Vendier, *Eur. J. Inorg. Chem.*, 2009, 3801.

View Article Online
DOI: 10.1039/C7DT04293K

38 S. J. Hawkes, *J. Chem. Educ.*, 1996, **73**, 516.
39 R. Maurice, L. Vendier, J. P. Costes, *Inorg. Chem.*, 2011, **50**, 11075.
40 E. Colacio, J. Ruiz, A. J. Mota, M. A. Palacios, E. Cremades, E. Ruiz, F. J. White, E. K. Brechin, *Inorg. Chem.*, 2012, **51**, 5857.
41 M. Evangelisti, F. Luis, L. J. de Jongh, M. Affronte, *J. Mater. Chem.*, 2006, **16**, 2534.
42 F. Cimpoesu, F. Dahan, S. Ladeira, M. Ferbinteanu, J. P. Costes, *Inorg. Chem,* 2012, **51**, 11279.
43 T. Yamaguchi, J. P. Costes, Y. Kishima, M. Kojima, Y. Sunatsuki, N. Bréfuel, J. P. Tuchagues, L. Vendier, W. Wernsdorfer, *Inorg. Chem.*, 2010, **49**, 9125.
44 L. Ungur, M. Thewissen, J. P. Costes, W. Wernsdorfer, L. F. Chibotaru, *Inorg. Chem.*, 2013, **52**, 6328.
45 (a) A. Hosoi, Y. Yukawa, S. Igarashi, S. J. Teat, O. Roubeau, M. Evangelisti, E. Cremades, E. Ruiz, L. A. Barrios, G. Aromí, *Chem. Eur. J.*, 2011, **17**, 8264. (b) T. N. Hooper, J. Schnack, S. Piligkos, M. Evangelisti, E. K. Brechin, *Angew. Chem. Int. Ed.*, 2012, **51**, 4633. (c) T. D. Pasatoiu, A. Ghirri, A. M. Madalan, M. Affronte, M. Andruh, *Dalton Trans.*, 2014, **43**, 9136. (d) T. N. Hooper, R. Inglis, G. Lorusso, J. Ujma, P. E. Barran, D. Uhrin, J. Schnack, S. Piligkos, M. Evangelisti, E. K. Brechin, *Inorg. Chem.*, 2016, **55**, 10535. (e) E. Guarda, K. Bader, J. van Slageren, P. Alborés, *Dalton Trans.*, 2016, **45**, 8566. (f) A. B. Canaj, M. Siczek, T. Lis, R. Inglis, G. Lorusso, M. Evangelisti, C. J. Milios, *Dalton Trans.,* 2017, **46**, 3449. (g) K. Griffiths, C. Harding, V. N. Dokorou, E. Loukopoulos, S. I. Sampani, A. Abdul-Sada, G. J. Tizzard, S. J. Coles, G. Lorusso, M. Evangelisti, A. Escuer, G. E. Kostakis, *Eur. J. Inorg. Chem.*, 2017, **33**, 3938.
46 (a) J.-B. Peng, Q.-C. Zhang, X.-J. Kong, Y.-P. Ren, L.-S. Long, R.-B. Huang, L.-S. Zheng, Z. Zheng, *Angew. Chem. Int. Ed.*, 2011, **50**, 10649. (b) Y.-Z. Zheng, M. Evangelisti, R. E. P. Winpenny, *Angew. Chem. Int. Ed.*, 2011, **50**, 3692. (c) S. Zhang, P. Cheng, *ChemPlusChem*, 2016, **81**, 811.

View Article Online
DOI: 10.1039/C7DT04293K

Ni^{II}-Ln^{III} complexes with o-vanillin as main ligand: Syntheses, structures, magnetic and magnetocaloric properties

Synopsis

Ortho-vanillin yields three types of heteronuclear Ni^{II}-Ln^{III} complexes, going from dinuclear to tetranuclear defect dicubane complexes.